

AMERICAN UNIVERSITY OF BEIRUT

SOLAR CHIMNEY COMBINED WITH PASSIVE
EVAPORATIVE COOLER APPLIED ON GLAZING
SURFACES

by
ALBERT GEORGES AL TOUMA

A thesis
submitted in partial fulfillment of the requirements
for the degree of Master of Engineering
to the Department of Mechanical Engineering
of the Faculty of Engineering and Architecture
at the American University of Beirut

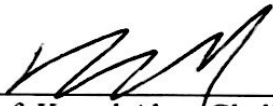
Beirut, Lebanon
April 2016

AMERICAN UNIVERSITY OF BEIRUT

SOLAR CHIMNEY COMBINED WITH PASSIVE
EVAPORATIVE COOLER APPLIED ON GLAZING
SURFACES

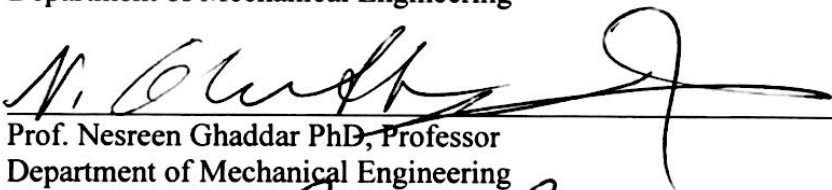
by
ALBERT GEORGES AL TOUMA

Approved by:



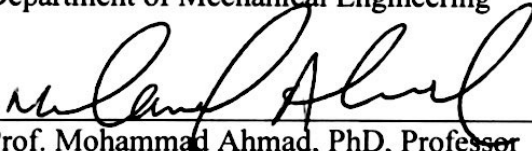
Prof. Kamel Abou Ghali, PhD, Professor
Department of Mechanical Engineering

Advisor



Prof. Nesreen Ghaddar PhD, Professor
Department of Mechanical Engineering

Co-Advisor



Prof. Mohammad Ahmad, PhD, Professor
Department of Chemical and Petroleum Engineering

Member of Committee

Date of thesis defense: April 20, 2015

AMERICAN UNIVERSITY OF BEIRUT

THESIS, DISSERTATION, PROJECT RELEASE FORM

Student Name: Al Touma Albert Georges
Last First Middle

Master's Thesis

Master's Project

Doctoral Dissertation

I authorize the American University of Beirut to: (a) reproduce hard or electronic copies of my thesis, dissertation, or project; (b) include such copies in the archives and digital repositories of the University; and (c) make freely available such copies to third parties for research or educational purposes.

I authorize the American University of Beirut, **three years after the date of submitting my thesis, dissertation, or project**, to: (a) reproduce hard or electronic copies of it; (b) include such copies in the archives and digital repositories of the University; and (c) make freely available such copies to third parties for research or educational purposes.



Signature

April 26 2016

Date

ACKNOWLEDGMENTS

I would like to express my deepest gratitude for Prof. Kamel Abou Ghali for his advisory, guidance and patience through my graduate study.

I would also like to thank Prof. Nesreen Ghaddar for her recommendations, thoughtful ideas and help in completing this work.

Special thanks to Prof. Mohammad Ahmad for being a member of my thesis committee.

I would also like to show deep gratitude and appreciation to my family members and friends for their support throughout the past years.

AN ABSTRACT OF THE THESIS OF

Albert Georges Al Touma: for Master of Engineering
Major: Mechanical Engineering

Title: Solar Chimney Integrated with Passive Evaporative Cooler Applied on Glazing Surfaces

This study investigates the performance of a hybrid system applied on glazing surfaces in reducing the space cooling load and radiation asymmetry. The proposed system combines the principles of passive evaporative cooling with the natural buoyant flow in solar chimneys to entrain outdoor air and attenuate the window surface temperature. A predictive mathematical heat and mass model combining the evaporative cooler, glazing section, solar chimney and an office space is developed to study the performance of the proposed system in harshly hot climates. The developed model was validated through experiments conducted in a twin climatic chamber for certain temperature, humidity and solar radiation conditions. Good agreement was found between the measured and predicted temperatures and thermal loads where the maximum discrepancy was to 4.3%.

The proposed system is applied in a case study on a typical office space to analyze its effectiveness in terms of decreasing the window temperature, and subsequently the space load and radiation asymmetry, while maintaining the indoor conditions and requirements. Results have shown that the system was capable of reducing the space load by 19.4% and attenuating the radiation asymmetry significantly during the working hours of the day for office spaces having window-to-wall ratios of 40% in Riyadh, KSA. The system performance diminished when applied in locations suffering from humid weather climates.

CONTENTS

| | |
|--|------|
| ACKNOWLEDGMENTS..... | v |
| ABSTRACT..... | vi |
| NOMENCLATURE..... | ix |
| LIST OF ILLUSTRATIONS..... | x |
| LIST OF TABLES..... | xi |
| | |
| Chapter | Page |
| I. INTRODUCTION..... | 1 |
| II. SYSTEM DESCRIPTION..... | 4 |
| III. METHODOLOGY..... | 6 |
| A. System Mathematical Model..... | 6 |
| 1. Evaporative Cooler | 7 |
| 2. Glazing Section | 8 |
| 3. Solar Chimney | 10 |
| 4. Flow Model..... | 11 |
| 5. Applicability of Model | 11 |
| B. Space Model..... | 13 |
| C. Radiation Asymmetry | 13 |
| D. Numerical Solution Methodology..... | 14 |
| III. EXPERIMENT..... | 16 |
| IV. RESULTS AND DISCUSSION..... | 22 |
| A. Model Validation | 22 |
| B. Case Study..... | 24 |

| | |
|--|-----------|
| 1. System Application in Dry Conditions (Riyadh) | 26 |
| 2. System Application in Dry Conditions (Riyadh)..... | 29 |
| III. CONCLUSION..... | 32 |
| BIBLIOGRAPHY..... | 35 |

NOMENCLATURE

| | |
|-----------|--|
| c_p | Specific Heat (J/kg·K) |
| F | View Factor |
| f | Friction Loss Coefficient |
| g | Gravity (m/s ²) |
| H | Height (m) |
| h_c | Heat convection coefficient (W/m ² ·K) |
| h_m | Mass convection coefficient (m/s) |
| h_{fg} | Latent Heat of Water (J/kg) |
| k | Thermal Conductivity (W/m·K) |
| \dot{m} | Mass Flow Rate (kg/s) |
| Q | Solar radiation (W/m ²) |
| q_{rad} | Radiative heat exchange with the space (W/m ²) |
| T | Temperature (°C) |
| t | Thickness (m) |
| u | Velocity (m/s) |
| W | Width (m) |
| w | Humidity ratio (kg/kg) |
| w^* | Humidity ratio of saturated air (kg/kg) |
| y | Height position (m) |

Greek Symbols

| | |
|---------------|---|
| ρ | Density (kg/m ³) |
| α | Surface Absorptivity |
| τ | Surface Transmissivity |
| ε | Surface Emissivity |
| σ | Stefen Boltzmann constant (W/m ² ·K ⁴) |
| β | Buoyancy Flux (m ⁴ /s ³) |

Subscripts

| | |
|-----|-------------|
| c | Convection |
| ch | Chimney |
| i | In |
| m | Mass |
| o | Out |
| og | Outer Glass |
| r | Radiation |
| wat | Water |

ILLUSTRATIONS

| Figure | | Page |
|--------|---|------|
| 1. | (a)Schematic of the proposed system and (b) air property changes on the psychrometric chart..... | 5 |
| 2. | Schematic of the evaporative cooler | 7 |
| 3. | Schematic of the glazing section | 7 |
| 4. | Algorithm for solving the integrated system | 15 |
| 5. | Schematic of the experimental setup in the twin climatic chamber..... | 16 |
| 6. | Experimental preparation of the proposed system | 18 |
| 7. | Installation of system on the window surface | 19 |
| 8. | Window inner surface temperature during the experiment with and without the system..... | 23 |
| 9. | Hourly distribution of the (a) Space load and (b) Window temperature with and without the system for Riyadh | 29 |
| 10. | Hourly distribution of the (a) Space load and (b) Window temperature with and without the system for Jeddah | 33 |

TABLES

| Table | | Page |
|-------|---|------|
| 1 | Properties of window and outer glass used in the experiment..... | 17 |
| 2 | Experimental and predicted energy savings of the system..... | 22 |
| 3 | Experimental and predicted air velocity and temperatures in the system..... | 23 |
| 4 | Experimental and predicted temperatures of the outer, the window and the walls..... | 24 |
| 5 | Space envelope used in the case study..... | 25 |
| 6 | Temperature and relative humidity profiles in Riyadh and Jeddah.... | 25 |
| 7 | Comparison between predicted and actual solar radiation data available in literature..... | 26 |

CHAPTER I

INTRODUCTION

Designing large glazing areas has become an essential feature of modern architecture and very common in office spaces. They improve the building's aesthetics, enhance the visual comfort by transmitting more natural lighting and increase the productivity of workers due to the bright working environment. This even led to the design of buildings with fully-glazed facades. However, among all the components of the building envelope, glazed surfaces are the most critical due to their weak thermo-physical properties that are easily overcome by outdoor conditions [1], and have been proven to account for 39% of the building energy performance [2].

The space load portion caused by windows is of two types; radiation transmitted through the window transparent surface and heat dissipated by solar absorption. The transmitted radiation is absorbed by the internal surfaces and causes an increase in the space air temperature and cooling load. On the other hand, the absorbed solar radiation causes a further increase in the window temperature leading to an asymmetrical radiative environment where thermal comfort requirements are sacrificed due to the exposure to high surface temperatures [3]. Reducing the space load and resulting radiation asymmetry due to windows was studied by many researchers. Antoun et al. [4] tackled this problem by changing the air distribution system to coaxial personalized ventilation. The ability of the system to localize air mitigated the thermal tension and uncomfortable sensation due to the radiative asymmetrical field and led to 36% of energy savings when compared to a mixing ventilation system. However,

changing the air distribution system is not easily retrofitted in buildings and inevitably costly to implement.

Alternatively, the window performance and its effect on energy consumption has become a hot research topic. Kontoleon [5] studied different methods on reducing solar transmission through windows by considering the building orientation and facades on which windows are installed. It was found that up to 25% of the cooling energy is saved when the fully-glazed façade orientation is changed to the north direction. Nonetheless, the technique of changing the window orientation is unfeasible in existing buildings and may be practical to new buildings only. Other researchers have considered changing the window materials to ameliorate its performance. Some found that traditional absorptive glazing materials available in the colors of bronze and grey [6], vanadium dioxide thermochromic glass windows [7] and near-infrared electrochromic glass windows [8] managed to reduce solar radiation transmission and diminish the cooling energy consumption. In fact, windows with enhanced thermal and optical properties for reductions in heat and radiation entrance were found to reduce the cooling energy index by 40% in office spaces [9]. Moreover, heat passage through triple and quadruple pane windows has also been studied through computational fluid flow analysis and it was found that using multiple pane windows slows down the flow in the window cavities and also acts as a radiation shield resulting in large energy savings [10]. Additionally, the effect of adding phase-change materials (PCM) to windows on the dynamic heat transfer was found to reduce the heat entering the building by 18.3% for a typical summer day in China [11]. Although these alternative research methods have improved the window performance and managed to reduce the radiation and heat entrance to the space, they either do not incorporate passive systems or are expensive to

adopt and unsustainable on the long run. This is why searching for alternative passive techniques for reducing the window temperature was deemed necessary.

One promising passive technique to reduce the window surface temperature was the design of single and dual airflow windows [12-14]. These windows allow air passage through their cavities and use solar heat as the driving force. During cooling seasons, indoor air driven by buoyant forces is entrained into the window cavity to reduce its surface temperature before getting exhausted. Yet, this mode imposes additional ventilation load of fresh air to the space to compensate for the air exhausted through the window. On the other hand, avoiding extra ventilation load is achieved by introducing windows with outdoor air curtain mode where moderate outdoor air is entrained into the window cavity to attenuate any increase in its surface temperature. However, this raises several limitations on the effective operation of this mode at high outdoor temperatures. In places where outdoor temperatures are very high, any heat exchange with outdoor air does not diminish the window temperature and may eventually have a counter effect in increasing the space cooling load.

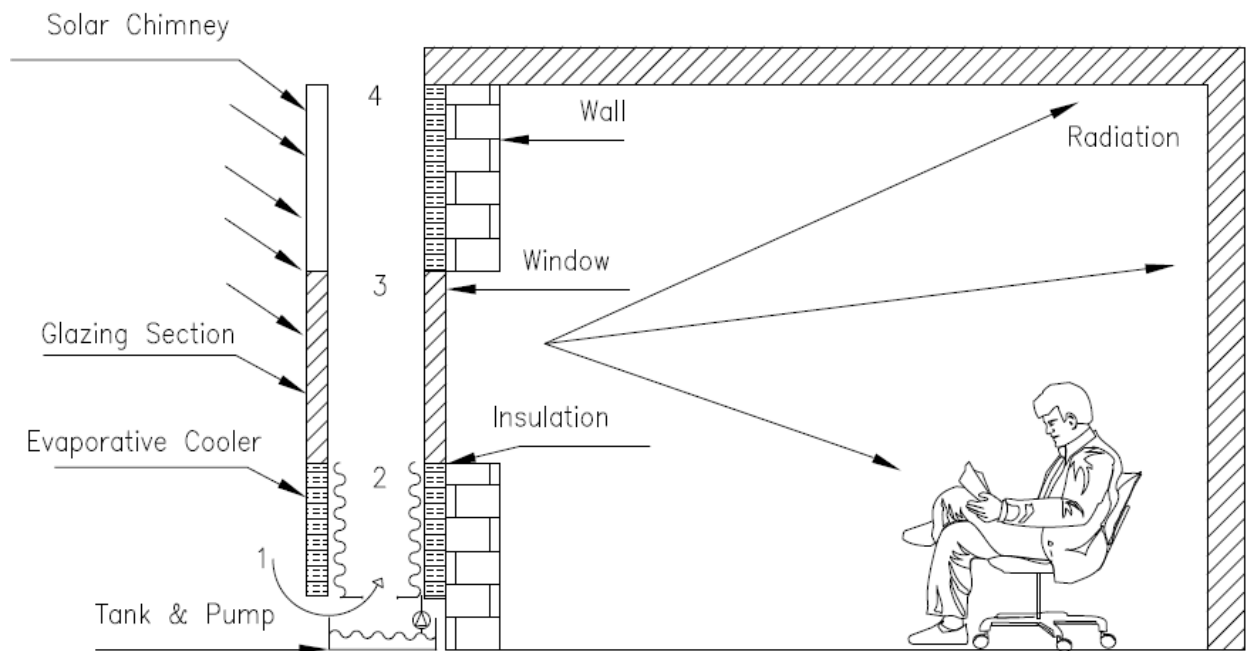
Consequently, this problem highlights the need for innovative passive design strategies to enhance reductions in the temperature of glazing surfaces with no additional ventilation or energy demands. These strategies should be feasible in existing buildings and practically applicable in countries suffering from hot climates. In this study, the proposed research system is a combination of a passive evaporative cooler and a solar chimney and provides means of reducing the window temperature by cooling its surface through natural flow of outdoor air. A numerical model for the entire system is developed, validated experimentally and applied in a case study to assess its effectiveness in reducing the space cooling load and radiation asymmetry.

CHAPTER II

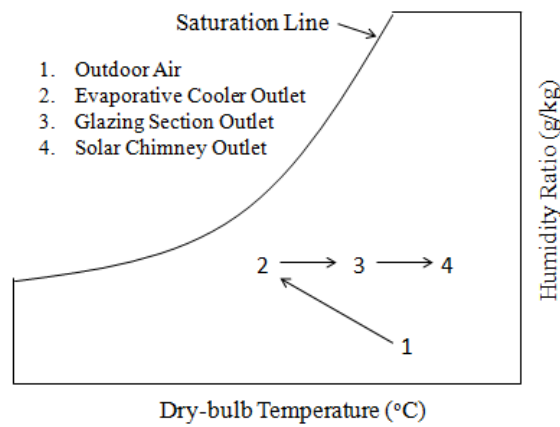
SYSTEM DESCRIPTION

The proposed system is composed of three main components; evaporative cooler, glazing section and solar chimney located consecutively above each other and applied on windows in typical office spaces as shown in **Fig. 1(a)**. The solar chimney, which is composed of an absorptive material on the outer side and insulated on the back side, drives the airflow in the entire channel; as it is heated by solar radiation, buoyancy raises the air due to stack effect. As air is being dragged upwards, it passes through the evaporative cooler and the glazing section located respectively below and in front of the window. The evaporative cooler consists of a vertical rectangular channel with four water absorbing sheets installed along its height as well as a small reservoir and a pump that ensure continuous water supply to these sheets. The evaporative cooler is also insulated from the outer surfaces to eliminate the effect of solar radiation. The glazing section consists of the window installed in a space and an outer glazing layer installed in front of it and closed on both sides so that air can freely move in the vertical direction only.

The whole psychrometric process of the air in the proposed system is shown in **Fig. 1(b)**. Outdoor air at State 1 enters the evaporative cooler where it is cooled and humidified simultaneously as it exchanges heat and mass with the water sheets until it reaches State 2 at the inlet of the glazing section. As air passes through this section, it extracts heat from the outer glass and window surfaces and reaches State 3. Then, air enters the solar chimney where it extracts more heat before getting exhausted out of the entire system at State 4.



(a)



(b)

Fig. 1: (a) Schematic of the proposed system and (b) air property changes on the psychrometric chart.

CHAPTER III

METHODOLOGY

In order to study the performance of the proposed system, a simplified one-dimensional steady-state heat and mass model in the direction of the air flow is developed. Thus, the differential form of heat and mass equations is used in the air gap. Also, the model assumes constant temperatures along the height of window and outer glass surfaces which results in the use of the integral form in the energy balance equations. The developed model couples the evaporative cooler, glazing section, solar chimney and the space to predict the window and walls' temperatures, space total load and radiant temperature asymmetry with respect to an occupant located at a certain position in the space.

A. System Mathematical Model

The proposed model for the entire channel considers forced convection in the evaporative cooler and glazing section and free natural convection in the solar chimney. This consideration is checked by ensuring that the ratio of Grashof number of Reynolds number squared is less than 0.1 in the evaporative cooler and glazing section. Thus, the flow does not suffer from any buoyancy effect caused by downward air circulation in the evaporative cooler due to cooling surfaces and upward air motion in the glazing section due to heated surfaces. In addition, the model assumes a channel width much larger than its gap, which allows treating the system as air flow between two parallel plates [15].

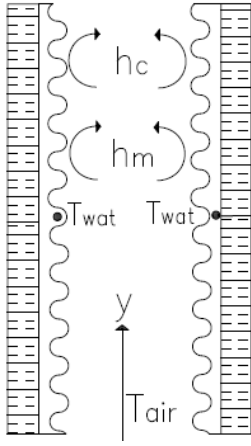


Fig. 2: Evaporative cooler.

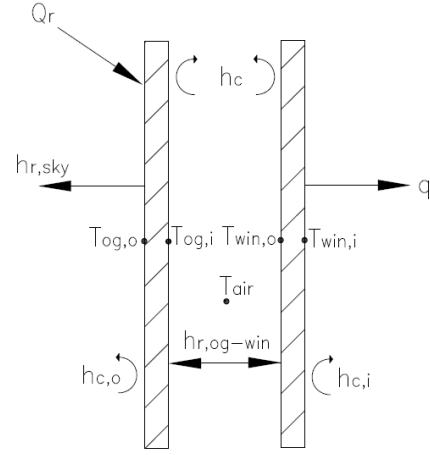


Fig. 3: Glazing section.

1. Evaporative Cooler

A schematic of the evaporative cooler is shown in **Fig. 2**. As air is going up, it exchanges mass through convection with the four water absorbing sheets installed along its height. Following Miyazaki et al. [16] and Itani et al. [17] models, the mass balance equation of the air in this section is given by:

$$\rho_{air} u_{air} t_{gap} \frac{dw_{air}}{dy} = 2 \times \rho_{air} h_m (w^* - w_{air}) \quad (1)$$

In Eq. (1), the left hand side represents the mass flux to the fluid whereas the right hand side represents the convective moisture gain of the passing air where t_{gap} is the thickness of the channel gap, h_m is the convection mass transfer coefficient and w^* is the humidity ratio of saturated air at water temperature. Similarly, the passing air exchanges heat with these sheets through convection. The passing air exchanges heat with these sheets through convection. The heat balance equation of the air is expressed by [18]:

$$\rho_{air} c_{p,air} u_{air} t_{gap} \frac{dT_{air}}{dy} = 2 \times h_c (T_{wat} - T_{air}) + 2 \times \rho_{air} h_m h_{fg} (w_{air} - w^*) \quad (2)$$

The left hand side of Eq. (2) is the heat flux to the fluid whereas the right hand side terms represent the convective sensible and latent heat losses of air in the channel. In Eq. (2), h_c is the convection heat transfer coefficient, h_{fg} is the latent heat of water and T_{wat} is the water sheets temperature assumed to be constant due to continuous water supply. In Eqs. (1)-(2), the convection coefficients are calculated using Gnielinski correlation for Nusselt number^{17,18} which is valid over a large range of Reynolds number including the transition region [15]. Assuming a Lewis number of unity [16-19]:

$$h_m = \frac{h_c}{\rho_{air} \times c_{p,air}} \quad (3)$$

2. Glazing Section

As shown in **Fig. 3**, the glazing section is divided into three main layers: the outer glass, air and window layers. Energy balance equations are carried out for each of them to solve for the outer glass and window outer ($T_{og,o}$, $T_{win,o}$) and inner ($T_{og,i}$, $T_{win,i}$) surface temperatures as well as the air layer temperature distribution (T_{air}) [16-19].

These energy balances consider radiation absorbed and transmitted by surfaces, radiation exchange between surfaces, conduction through the outer glass and window as well as the convection of outdoor, induced and indoor air with different surfaces.

For the outer glass both outer and inner surfaces, energy balances are given respectively by:

$$\alpha_{og} Q_r + h_{c,o} (T_o - T_{og,o}) + h_{r,sky} (T_{sky} - T_{og,o}) + \frac{k_{og}}{t_{og}} (T_{og,i} - T_{og,o}) = 0 \quad (4)$$

$$\frac{1}{H_{og}} \int_0^{H_{og}} h_c (T_{air} - T_{og,i}) .dy + h_{r,og-win} (T_{win,o} - T_{og,i}) + \frac{k_{og}}{t_{og}} (T_{og,o} - T_{og,i}) = 0 \quad (5)$$

The airflow energy balance is given by

$$\rho_{air} c_{p,air} u_{air} t_{gap} \frac{dT_{air}}{dy} = h_c (T_{og,i} - T_{air}) + h_c (T_{win,o} - T_{air}) \quad (6)$$

The energy balances for the window outer and inner surfaces are given respectively by

$$\tau_{og} \alpha_{win} Q_r + \frac{1}{H_{win}} \int_0^{H_{win}} h_c (T_{air} - T_{win,o}) .dy + h_{r,og-win} (T_{og,i} - T_{win,o}) + \frac{k_{win}}{t_{win}} (T_{win,i} - T_{win,o}) = 0 \quad (7)$$

$$h_{c,i} (T_i - T_{win,i}) + q_{rad} + \frac{k_{win}}{t_{win}} (T_{win,o} - T_{win,i}) = 0 \quad (8)$$

In Eqs. (4)-(8), subscripts o and i denote the outer and inner surfaces where α is the absorptivity, τ is the solar transmissivity, k is the thermal conductivity and Q_r is the solar radiation intensity hitting the window vertical surface. The second term q_{rad} is the radiation exchange between the window and indoor space components including walls, ceiling and floor and is expressed as [20, 21]:

$$q_{rad} = \sum_{i=i}^n F_{win-wall(i)} \varepsilon \sigma (T_{win}^4 - T_{wall(i)}^4) \quad (9)$$

where F is the view factor between two surfaces, ε is the multiple of the emissivities of the surfaces and n is the total number of surfaces. The radiation heat transfer

coefficients $h_{r,sky}$ and $h_{r,og-win}$ are expressed as [16]:

$$h_{r,sky} = F_{og-sky} \varepsilon_{og} \sigma (T_{sky} + T_{og}) (T_{sky}^2 + T_{og}^2) \frac{(T_{sky} - T_{og})}{(T_o - T_{og})} \quad (10)$$

$$h_{r,og-win} = \frac{F_{og-win} \sigma (T_{og} + T_{win}) (T_{og}^2 + T_{win}^2)}{\frac{1}{\varepsilon_{og}} + \frac{1}{\varepsilon_{win}} - 1} \quad (11)$$

Hagishima et al. [22] model for the calculation of the convection heat transfer coefficient on vertical wall surfaces with the outer environment using the wind velocity is adopted:

$$h_{c,o} = 10.21 \times u_{wind} + 4.47 \quad (12)$$

The sky temperature is calculated in terms of the outdoor dry-bulb temperature, dew-point temperature and hour time using Duffie and Beckman model [23]:

$$T_{sky} = T_o [0.711 + 0.0056 \times T_{dp} + 0.000073 \times T_{dp}^2] + 0.013 \times \cos(15 \times hr)]^{1/4} \quad (13)$$

Since forced convection dominates on the glazing section and Reynolds number falls within the transition range, Gnielinski correlation for Nusselt number is also used to calculate the heat transfer coefficient of induced air with the outer glass and window surfaces [15].

3. Solar Chimney

The solar chimney section is treated in a similar manner. By insulating the back of the chimney and neglecting conduction through its surface material due to small Biot number, energy equations for the solar chimney surface (T_{ch}) and induced air (T_{air}) only are carried out [16-19].

For the chimney surface:

$$\alpha_{ch} Q_r + h_{c,o} (T_o - T_{ch}) + h_{r,sky} (T_{sky} - T_{ch}) + \frac{1}{H_{ch}} \int_0^{H_{ch}} h_c (T_{air} - T_{ch}) . dy = 0 \quad (14)$$

For the airflow:

$$\rho_{air} c_{p,air} u_{air} t_{gap} \frac{dT_{air}}{dy} = h_c (T_{ch} - T_{air}) \quad (15)$$

Since flows in solar chimneys are dominated by free natural convection, Nusselt number for this section is found by the empirical correlations for free convective flows

between parallel plates subjected to constant heat flux on one side and adiabatic on the other side [15].

4. Flow Model

For a vertical chimney that ensures unidirectional upward flow, the flow model of Chen et al. [24-26] is adopted. This model predicts the flow induced by buoyancy between two parallel plates subjected to constant heat flux on one side only by the balance between stack pressure and pressure loss along the chimney. The energy equation in the air layer is substituted in the correlation of stack pressure to account for the external heat flux and the induced mass flow rate is then calculated according to:

$$\dot{m} = [2 \times (\frac{t_{gap}^3 W^3 H \rho^2 g \beta}{f \times c_p}) Q_r]^{1/3} \quad (16)$$

In Eq. (16), W and H are the chimney width and height, g is the gravitational force, β is the thermal expansion coefficient and f is the friction loss coefficient along the chimney [24-26].

5. Applicability of Model

The applicability of the model is dependent on the prevention of the downward circulative flow close to the cooling surfaces. In order to prevent this from occurring, a mathematical analysis is carried out to find the dependence of the chimney height on the heat flux hitting the chimney surface and the temperature drop inside the evaporative cooler. The analysis starts by assuming that forced convection dominates over buoyancy in the evaporative cooler (i.e. $Gr/Re^2 < 0.1$), which leads to the following inequality:

$$\frac{g \beta t_{gap} \times \Delta T_{evap, cooler}}{u^2} < 0.1 \quad (17)$$

By substituting the velocity by the mass flow rate over the cross-sectional area, this inequality leads to:

$$Q_r^{2/3} \times H_{ch}^{2/3} \geq a \times \Delta T_{evap,cooler} \times t_{gap} \quad (18)$$

Where a is given in Eq. (17):

$$a = \frac{10 \times (g \times \beta)^{1/3} (\rho \times f \times c_p)^{2/3}}{2^{2/3}} \quad (19)$$

Therefore, in order to ensure a unidirectional upward flow, Eqs. (18)-(19) imply that the design of the chimney should be such that its height is greater than a critical value given by the following inequality:

$$H_{ch} \geq \frac{(a \times \Delta T_{evap,cooler} \times t_{gap})^{3/2}}{Q_r} \quad (20)$$

This critical value depends on the solar chimney air gap, the temperature difference in the evaporative cooler, the solar heat flux, the gravitational force, the fluid properties, and the friction loss coefficient along the chimney height. As natural and forced convections are proportional to the third and second powers of the air gap size respectively, increasing the air gap size favorites more the natural convection effect in the evaporative cooler. Thus, this demands larger chimney heights so that forced convection overcomes the increase of natural convection in this section. Also, Eq. (18) implies that any increase in the temperature difference along the evaporative cooler should be counter-balanced by an increase in the solar chimney height. Yet, when significant solar heat flux hits the chimney surface, it induces larger natural convection effect along the entire channel which limits the importance of the chimney height. The air thermal properties and the friction loss coefficients also play an important role in satisfying this condition such that the thermal properties, which depend on its

temperature, as well as the friction losses demand larger solar chimney height to overcome the natural convection effect.

B. Space Model

The space model is crucial for the evaluation of the space cooling load and radiation asymmetry. The space model should be able to solve for the walls' inner surface temperatures at any time given the internal loads, outdoor ambient conditions and building envelope materials. The space model of Yassine et al. [20] is adopted; each wall is considered as multi-layers that are discretized in space and time to predict the temperature distribution every hour along these layers using the implicit numerical scheme.

C. Radiation Asymmetry

At a certain location in the space, the Radiant Temperature Asymmetry (RTA) is found by virtually dividing the space horizontally or vertically into two spaces and calculating the difference in their Radiant Temperatures (RT) [27]:

$$\Delta T_{RTA} = |T_{RT,1} - T_{RT,2}| \quad (21)$$

Assuming the same emissivity for all surfaces, the radiant temperature of each space is expressed as [21, 27]:

$$T_{RT} = \sum_{j=1}^n F_{i-j} \times T_j \quad (22)$$

In Eq. (22), F_{i-j} is the view factor of the i -th surface toward the j -th surface where i denotes the virtual plane, n is the total number of surfaces in each space and T_j is the temperature of the j -th surface in degrees Celsius.

D. Numerical Solution Methodology

The integrated model has been implemented in an algorithm whose sequence of operation is represented by the flow chart shown in **Fig. 4**. The algorithm input variables are the outdoor dry-bulb temperature, relative humidity and solar radiation. The space dimensions and internal heat loads as well as the system components' dimensions are all required as inputs to the coupled models.

Starting with initial arbitrary temperatures for the outer glass, window and walls, the flow model uses the outdoor driving conditions and assumes a chimney inlet temperature to estimate the flow in the entire channel. Using the upwind scheme, the heat and mass energy equations of the evaporative cooler are discretized into algebraic equations to solve for the air temperature and humidity distributions along its height. Then, the glazing section uses the outdoor conditions and space model, discretizes the air layer and undergoes an iterative process until the correct temperatures of the outer glass, induced air, window and walls are found with a maximum relative error of 10^{-4} for all grid points. Subsequently, the solar chimney uses the glazing section air outlet temperature and undergoes another iterative process for the chimney and air layers until the same temperature convergence criteria is met. Upon convergence, a correction of the chimney inlet air temperature in the flow model occurs and the same process is repeated until the correct inlet temperature is found with a maximum relative error of 10^{-4} . After the correct window temperature is found, the algorithm checks for the validity of the models and reuses the space model to calculate the space load and radiant temperature asymmetry.

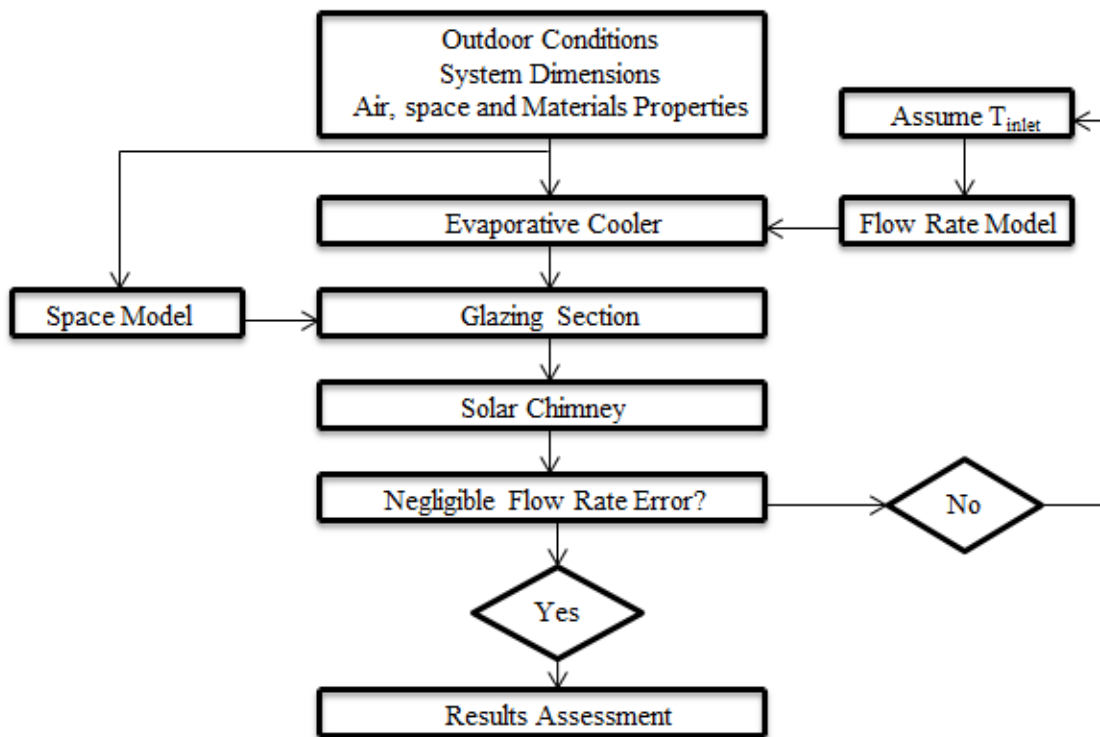


Fig. 4: Algorithm for solving the integrated model.

CHAPTER IV

EXPERIMENT

In order to validate the simulations performed for the integrated model, experiments were conducted in a twin climatic chamber. The system dimensions were chosen to guarantee unidirectional upward flow and experiments were carried out with and without the installation of the proposed system to assess its effectiveness in reducing the window temperature and space thermal load.

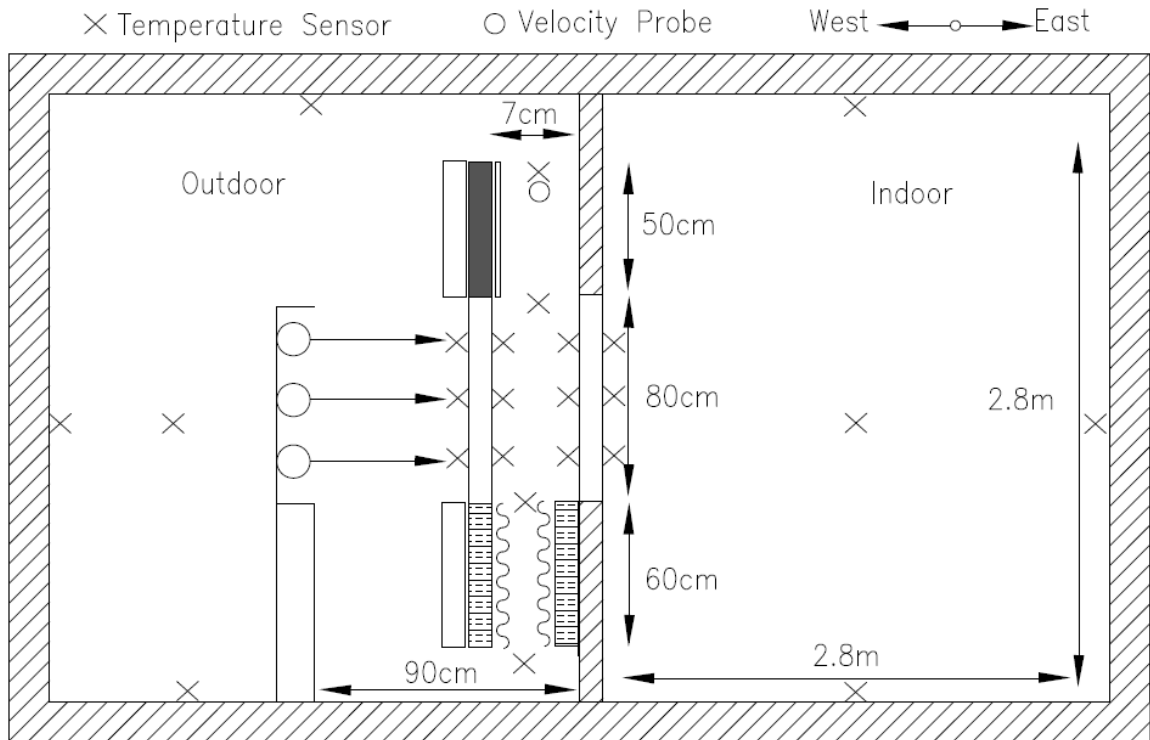


Fig. 5: Schematic of the experimental setup in the twin climatic chamber.

The chamber is composed of two rooms, each having a floor area of 7.84 m^2 and a height of 2.8 m, and are separated by a partition as shown in **Fig. 5**. The walls of the rooms were made of 10 cm thick polyurethane inside the chamber to minimize heat transfer and preserve the desired indoor conditions. One room was maintained at the

desired temperature using an electric chiller to represent typical indoor conditions during the summer. The chiller was set to provide 100% fresh air to the space at constant flow rate and different supply temperatures depending on the chilled water flow rate. The other room's temperature and humidity were fully-controlled to mimic the desired outdoor conditions. This room is also equipped with a fan to homogenize the air throughout the space. A clear single glazed window, which had a height and width of 0.8 m, was installed in the middle of the partition. The properties of the window are shown in Table 1.

Table 1: Properties of window and outer glass used in the experiment [28].

| Parameter | Value |
|-----------------------------|-------------------------|
| Thickness | 8 mm |
| Visible Transmittance | 0.87 |
| Visible Reflectance | 0.08 |
| Solar Heat Gain Coefficient | 0.8 |
| Thermal Conductivity | 5.17 W/m ² K |

The system components' dimensions have been carefully chosen to ensure the validity of the adopted models. The evaporative cooler was made of two 1 cm thick acrylic Plexiglas surfaces that are 0.6 m long and 0.8 m wide and separated by a gap of 7 cm. The water absorbing sheets were made of cotton fabric of high wicking capacity and were fixed along the height of the cooler using metallic meshes. As seen in **Fig. 6**, these meshes were also used to pass small nozzles that are connected to water sprays to ensure continuous supply of water throughout the experiment. The cooler's outer surface was then covered with 3.5 cm thick Styrofoam insulation. The glazing section consisted of the window, which was previously installed, and an outer glass layer made of the same materials and dimensions. The chimney was 0.5 m long and 0.8 m wide and was made of commercial 2 mm thick galvanized steel painted in matte black. Note that

the entire channel from the evaporative cooler to the solar chimney has been enclosed on the sides with Plexiglas covered with 3.5 cm of Styrofoam insulation.

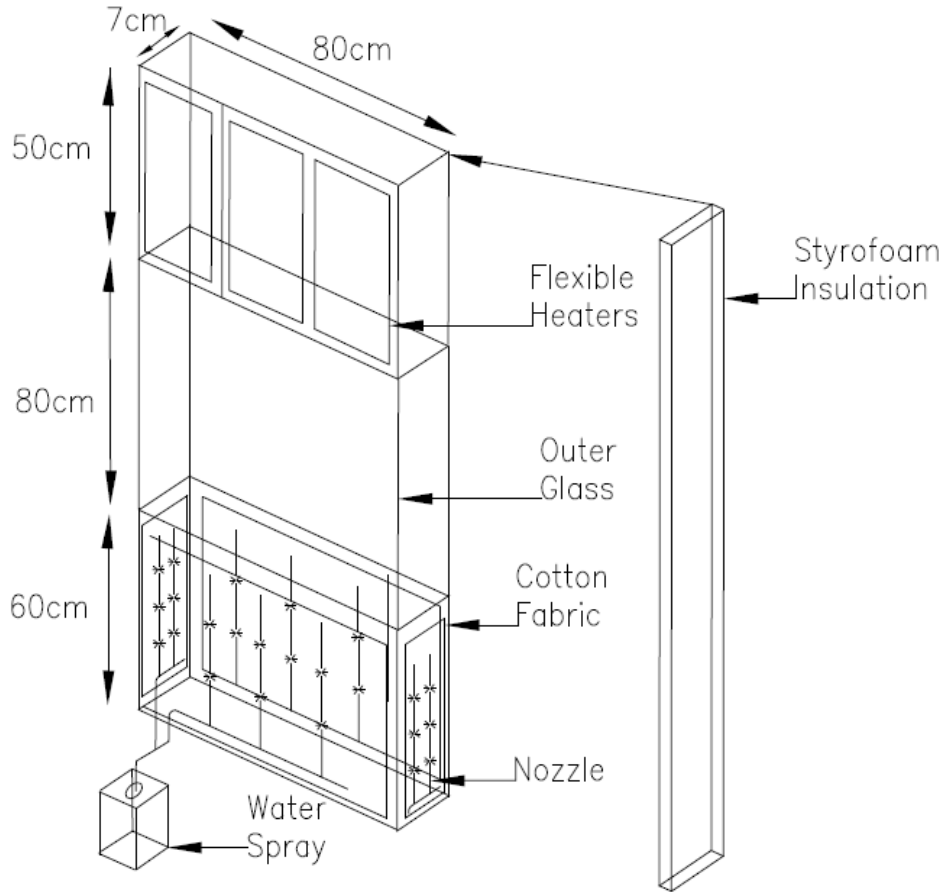


Fig. 6: Experimental preparation of the proposed system.

Six solar lamps of 1000 W each that provide light in the visible spectrum range were placed at a distance of 90 cm from the outer glass to simulate uniform solar radiation on the glazing section (**Fig. 5**). These lamps' power was controlled by dimmers as desired by the user and their solar intensity was measured at several locations of the window surface by a Huskeflux Pyranometer – LI-19 that has an accuracy of $\pm 1.8\%$. Reflectors have been placed behind the lamps to direct all of the light towards the glazing section. Since these lamps do not cover the height of the entire system, the chimney was chosen to be heated with uniform heat flux using

OMEGALUX flexible heaters that covered its whole inner surface. To maintain the same amount of heat flux on the window and chimney surfaces, these heaters were connected to a voltage regulator so that their power is controlled as desired. The chimney was then covered with Styrofoam insulation layer from outer side to direct all the heat towards the passing air as seen in **Fig. 7**.

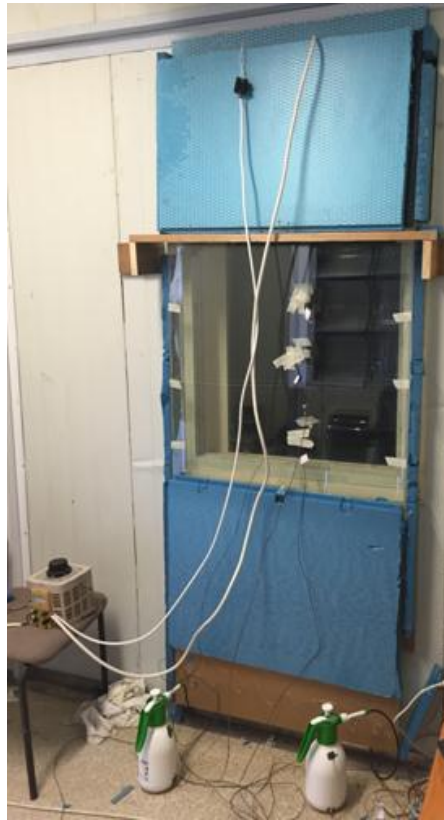


Fig. 7: Installation of system on the window surface.

The temperature and relative humidity of the air in the rooms were measured using BK PRECISION humidity/temperature meter with accuracies of ± 0.7 °C and $\pm 2.5\%$, respectively. Twelve K-type thermocouples were placed on both the window and the outer glass inner and outer surfaces at heights of 0.2 m, 0.4 m and 0.6 m and were connected to DAQPRO 5300 data logger for continuous temperature monitoring and

measurement. Similarly, K-type thermocouples were placed in the middle of each wall surface including the ceilings and the floors (**Fig. 5**). Radiation shields have been placed on all of these thermocouples to make sure that the temperature measurement is not affected by the radiation hitting the surfaces. In addition, five OMEGA Model HH21 thermometers of 0.1 °C resolution were used for the measurement of the air temperature at the outlets of the evaporative cooler, glazing section and solar chimney (**Fig. 5**), as well as the space supply and exhaust streams. All of these temperature sensors were calibrated to within ± 0.2 °C accuracy at a temperature of 0 °C. The airspeed inside the chimney was recorded by air velocity meter probe connected to OMEGA ANEMOMETER, which is a real-time data logger of a calibrated accuracy $\pm 5\%$ at 0.1 m/s. The probe was placed at the top of the chimney and at three different positions across its width: in the middle and 10 cm away from the edges. A similar probe was used to measure the air supply flow rate to the conditioned space.

To run the experiments, the first room was set to $28\text{ °C} \pm 0.7\text{ °C}$ with a relative humidity of $35\% \pm 2.5\%$ whereas the second room was maintained at $22\text{ °C} \pm 0.7\text{ °C}$ and $50\% \pm 2.5\%$. The solar lamps were regulated to provide a solar flux of $175\text{ W/m}^2 \pm 20\text{ W/m}^2$ on the window surface. These conditions were kept on for a long time; the temperatures were being continuously monitored until steady-state conditions have been reached where no significant variations were seen. In the second run, the system was added, the same temperature, relative humidity and solar radiation conditions were achieved and the flexible heaters voltage was adapted so that they provide an equal amount of heat flux to the chimney. Water was being sprayed to the evaporative cooler every 10-15 minutes until steady-state conditions were reached. The first experiment took 3-4 hours to reach steady-state whereas the second experiment took 5-6 hours. The

walls temperatures, space air supply and exhaust temperatures, induced air temperature at the outlets of the three different sections and the outer glass and window temperatures at the three different heights were all recorded where the uncertainty in the measurements was estimated to be less than ± 0.5 °C.

CHAPTER V

RESULTS AND DISCUSSION

A. Model Validation

During the experiments, the room, induced air and different surface temperatures at the aforementioned locations were monitored until steady-state conditions were reached. The space load was calculated by measuring the supply air flow rate to the space as well as the air supply and exhaust temperatures. In the first run when the system was not installed, the space load was 314 ± 3 W and the window had an average temperature of 28.7 ± 0.5 °C on its inner surface as seen in Table 2 and **Fig. 8**, respectively. The walls had temperatures of 28.0 ± 0.6 °C. After the installation of the system, the space load decreased to 301 ± 3 W, which is attributed to the reduction in the window temperature that decreased to 26.2 ± 0.5 °C (**Fig. 8**). The system showed negligible effect on the walls where the maximum change in their temperatures was less than 1.0 °C. Hence, the system was experimentally capable of reducing the space load and window inner surface temperature by 4.1% and 8.7%, respectively.

Table 2: Experimental and predicted energy savings of the system.

| Space Load | Without System (W) | With System (W) |
|-------------------|---------------------------|------------------------|
| Experiment | 314 \pm 5 | 301 \pm 5 |
| Simulation | 305 | 288 |

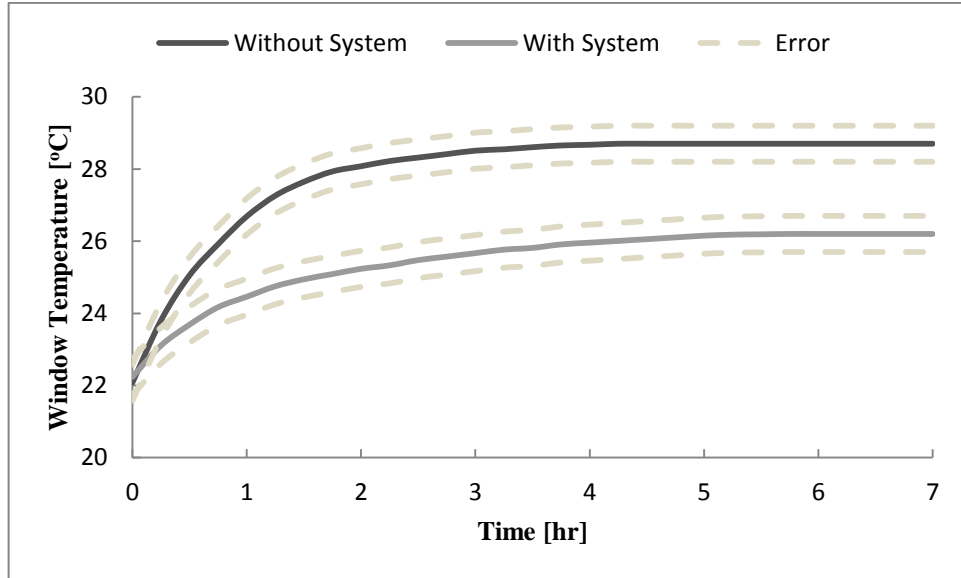


Fig. 8: Window inner surface temperature change during the experiment with and without the system.

In order to validate the experimental measurements, the same outdoor temperature, relative humidity and solar radiation conditions were used for the simulation. The physical dimensions and properties of the space envelope were also inputted to the algorithm and the simulation was performed over several hours for steady-state conditions to be satisfied. The experimental and simulation results of the integrated model are shown in Tables 2, 3, and 4. The experimental measurements presented in these tables take into consideration the uncertainties in the measuring devices.

Table 3: Experimental and predicted air velocity and temperature in the system.

| | Experiment | Simulation |
|---------------------------------------|-------------------|-------------------|
| Induced Mean Velocity (m/s) | 0.37 ± 0.02 | 0.42 |
| Evaporative Cooler Outlet (°C) | 25.3 ± 0.2 | 24.8 |
| Glazing Section Outlet (°C) | 26.8 ± 0.2 | 26.4 |
| Solar Chimney Outlet (°C) | 28.3 ± 0.2 | 27.9 |

As seen in Table 3, air at a velocity of 0.37 ± 0.02 m/s entered the evaporative cooler where it lost heat and reached a temperature of 25.3 ± 0.2 °C at its outlet. It then

entered the glazing section and solar chimney where it was heated by the window, outer glass and chimney surfaces before leaving at a temperature of 28.3 ± 0.2 °C. As depicted in Table 4, a 0.9 °C temperature difference was found between the window outer and inner surfaces. Good agreement was found between the experimental and simulation results for the temperatures and space load when the system was installed where the maximum discrepancy was 4.3%.

Table 4: Experimental and predicted temperatures of the outer glass, the window and the walls.

| Surface | Experiment Temperature (°C) | Simulation Temperature (°C) |
|----------------------------------|--|--|
| Outer Glass Outer Surface | 29.4 ± 1.1 | 28.4 |
| Outer Glass Inner Surface | 28.1 ± 0.9 | 27.3 |
| Window Outer Surface | 27.1 ± 0.9 | 26.8 |
| Window Inner Surface | 26.2 ± 0.9 | 26.1 |
| Ceiling | 27.5 ± 0.2 | 27.9 |
| Floor | 27.4 ± 0.2 | 27.9 |
| Window Opposite Wall | 28.2 ± 0.2 | 28.1 |
| Window Adjacent Wall 1 | 28.3 ± 0.2 | 28.0 |
| Window Adjacent Wall 2 | 28.7 ± 0.2 | 28.3 |

B. Case Study

In order to assess the performance of the proposed system in reducing the space load and radiation asymmetry, a case study of a typical office space located in the Kingdom of Saudi Arabia (KSA) was carried out. The office has a floor area of $6 \text{ m} \times 5 \text{ m}$ with a height of 2.8 m [17]. It consists of south and west facades exposed to the outside conditions whereas the remaining walls as well as the floor and ceiling are assumed to be partitioned with conditioned spaces. A window of dimensions $5.2 \text{ m} \times 1.3 \text{ m}$ is installed in the middle of the west façade (Window-to-Wall Ratio 40%). The space is maintained at a temperature of 22 °C and has two occupants [29] with working hours from 8 am to 6 pm where the internal heat load is caused by human occupancy

(100 W/person), computers (200W/computer) and lighting (10 W/m²) [4]. More information about the space envelope is shown in Table 5 according to the existing residential and commercial spaces in the Kingdom and following the energy conservation requirements of the Saudi Building Code [30-32].

Table 5: Space envelope used in the case study [28, 30-32].

| Parameter | Materials |
|-------------------|---|
| External Walls | 20 mm Plaster board + 20 cm CMU Medium weight + 20 mm Plaster board |
| Internal Walls | Gypsum board 32 mm |
| Floor and Ceiling | Light weight concrete 150 mm (U = 3.8 W/m ² .K) |
| Window | Single pane, single clear/tinted 8 mm |
| Outer Glass Type | Single clear glass 6 mm |

The evaporative cooler and solar chimney heights are considered to be 0.8 m with a channel gap of 5 cm. These dimensions were chosen to ensure that unidirectional upward flow in the channel dominates during the working hours of the day. July 21st was picked as a representative day of extreme summer conditions that typically range between June and August. The system was applied in Riyadh and Jeddah to mimic both dry and humid weather conditions. The cities' temperature and relative humidity profiles are shown in Table 6 [33].

Table 6: Temperature and relative humidity profiles in Riyadh and Jeddah, KSA [33].

| Time (hr) | Riyadh | | Jeddah | |
|-----------|------------------|-----------------------|------------------|-----------------------|
| | Temperature (°C) | Relative Humidity (%) | Temperature (°C) | Relative Humidity (%) |
| 8 | 34 | 13 | 31 | 55 |
| 9 | 36 | 13 | 32 | 52 |
| 10 | 38 | 12 | 34 | 41 |
| 11 | 40 | 12 | 35 | 32 |
| 12 | 41 | 11 | 35 | 34 |
| 13 | 42 | 10 | 35 | 34 |
| 14 | 44 | 8 | 36 | 34 |
| 15 | 44 | 8 | 37 | 32 |
| 16 | 45 | 7 | 38 | 30 |
| 17 | 44 | 8 | 37 | 30 |
| 18 | 43 | 9 | 36 | 32 |

The variation in the solar radiation hitting vertical surfaces is found for both cities using ASHRAE clear sky model [34]; this model calculates the direct, diffuse and reflected solar radiation in any orientation at any time of the day using the earth-sun angles as well as the solar angles. The results of this model are consistent with the most recent data found in literature for the year of 2013-2014, as shown in Table 7 [35].

Table 7: Comparison between predicted and actual solar radiation data available in literature [33].

| | ASHRAE Clear Sky Model | | Literature | |
|--|------------------------|--------|------------|--------|
| | Riyadh | Jeddah | Riyadh | Jeddah |
| Daily Direct Normal Irradiance (Wh/m²) | 9262 | 9074 | 9201 | 9481 |
| Daily Global Horizontal Irradiance (Wh/m²) | 7973 | 7889 | 8213 | 8084 |

The radiation asymmetry is analyzed with respect to an occupant who is considered to be seated one meter away from the center of the window [4]. The simulation was carried out for two cases; the first consisted of simulating the space alone without the system whereas the second consisted of simulating the space with the system installed on its window. In both cases, the simulation was done over several day cycles to eliminate the effect of initial conditions and the window temperature, the radiant temperature asymmetry and the space total load were then found.

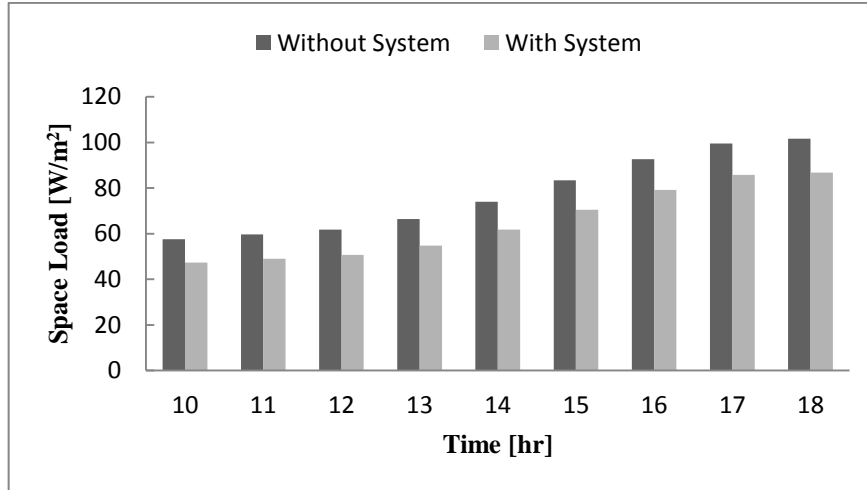
1. System Application in Dry Conditions (Riyadh)

The hourly distributions of the space load and window inner surface temperature for the two simulation cases when applied in Riyadh are shown in **Fig. 9**. The space total load when the system is not installed only affected by the outdoor temperature and solar radiation; it increases as they increase and ranged between 57.1 W/m² at 10 hours and 101.7 W/m² at 18 hour with an overall daily total gain of 1.27

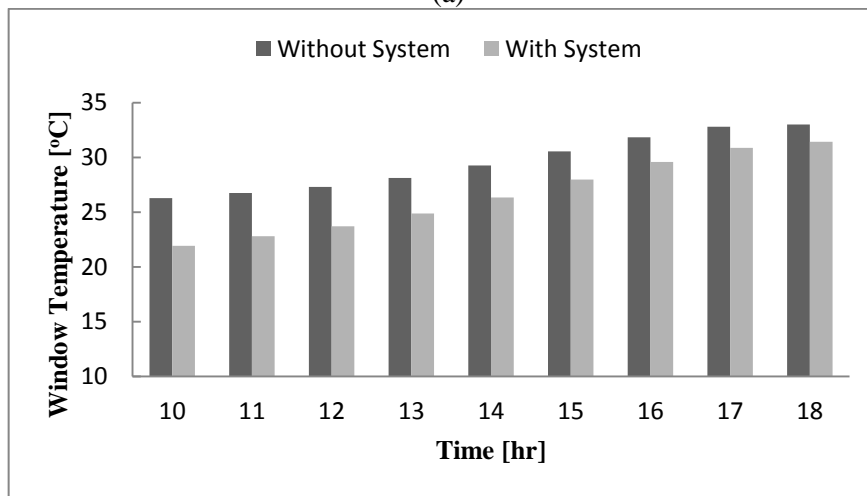
kWh/m². This load was found to be consistent with the monthly energy consumption found in Riyadh during the month of July as reported by Alaidroos et al. [31]. The temperature of the clear double pane window ranged between 26.3 °C at 10 hours and 33.0°C at 18 hours, as seen in **Fig. 9(b)**. The external and internal walls were at temperatures ranging between 23.2 °C and 29.4 °C and the radiant temperature asymmetry at the occupant's location ranged between 0.5°C at 10 hours 1.4 °C at 18 hours.

After the simulations were performed, the applicability of the model was checked to ensure accurate results. The model turned out to be valid at all times except at 6 hours when the solar radiation intensity was low and incapable of inducing an upward flow. At this hour, the 5 °C change in the air temperature inside the evaporative cooler was more significant than the moderate solar radiation applied on the chimney surface (less than 50 W/m²) for the chosen chimney height dimension. In between 6 and 19 hours, the window temperature was significantly reduced when the system was installed. Yet, the percentage reduction changed from one hour to another depending on the outdoor weather conditions; as more radiation hits the west façade, a larger flow is induced in the channel which improves the ability of the system to extract heat from the window surface. Additionally, at high temperature and solar radiation, the relative humidity profile reaches its lowest limits, which increases heat exchange in the evaporative cooler and also enhances the performance of the entire system. After the system was installed, the window temperature ranged between 21.9 °C and 31.4 °C. Consequently, the space load was reduced to range between 47.3 W/m² and 86.7 W/m² with the peak load reduced by 14.7% at 18 hours. Also, the walls' maximum temperature decreased to 28.4 °C leading to a moderation of the radiant temperature

asymmetry, especially between 8 and 14 hours when it was less than 0.4 °C. Hence, the system led to 19.8% overall reduction in the space total load throughout the day. The thermal gain through the window was reduced by 39%, which was found to be slightly larger than the reduction caused by the installation of the single airflow window with outdoor air curtain mode when applied in hot summer climates [13].



(a)



(b)

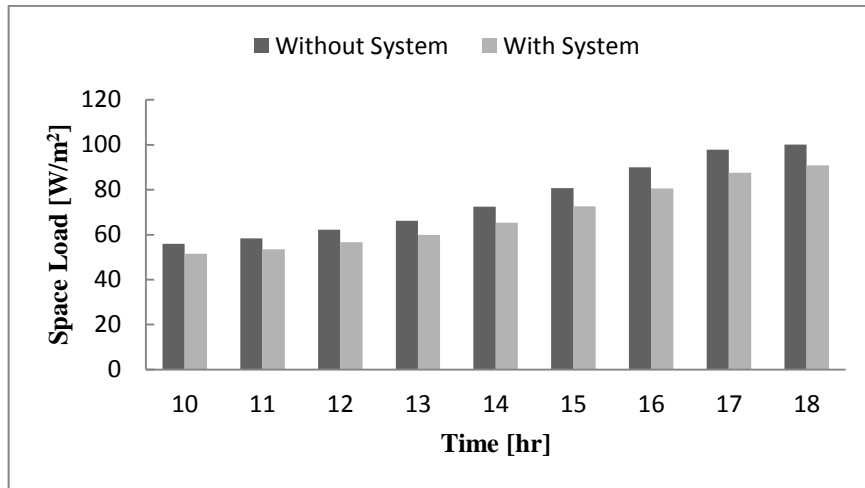
Fig. 9. Hourly distribution of the (a) Space load (b) Window temperature with and without the system for Riyadh.

2. System Application in Humid Conditions (Jeddah)

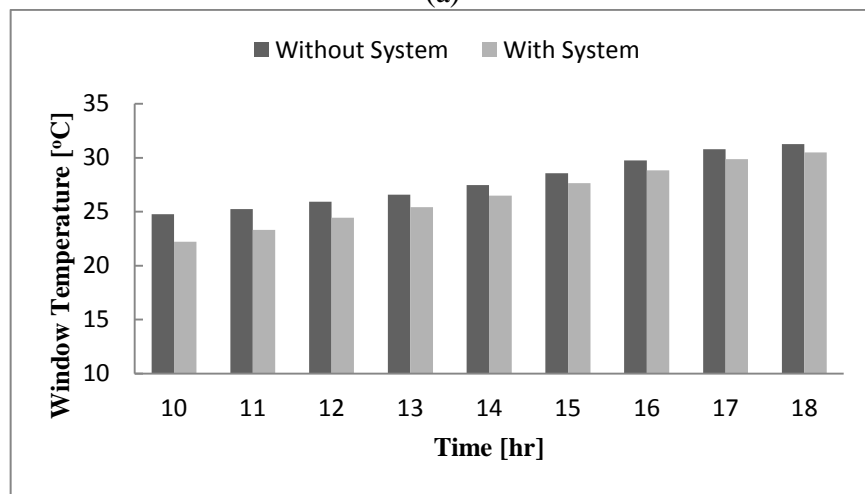
As the performance of the system in general and evaporative cooler in specific is highly dependent on the outdoor relative humidity, the original model was applied in the humid weather of Jeddah. As seen in **Fig. 10(a)**, the space total load when the system is not installed ranged between 56.0 W/m^2 at 10 hours and 100.1 W/m^2 at 18 hours. As reported by Alaidroos et al [31] and Zell et al [35], Riyadh and Jeddah have comparable monthly energy consumptions due closely similar temperature and solar radiation profiles. The temperature of the clear double pane window ranged between

24.8 °C at 10 hours and 31.3 °C at 18 hours, as depicted in **Fig. 10(b)**. The walls' temperatures were between 23.7 °C and 29.3 °C and the radiant temperature asymmetry reached 1.0 °C at 18 hours.

After the system is installed, the applicability of the model was also checked to ensure unidirectional upward flow in the channel. Similar to the case of Riyadh, the model turned out to fail at 6 hours when the small applied solar radiation was unable to overcome the 3-4 °C drop in the evaporative cooler. For the rest of the day, the reduction in window temperature when the system is installed was significantly affected by the outdoor relative humidity where the maximum decrease was less than 3.0 °C. This change is attributed to the moderate performance of the system at high relative humidity; higher humidity ratio leads to less latent heat exchange of outdoor air with the water sheets which render the air less capable of extracting heat from the window surface. These changes resulted in 9.3% decrease in the peak load that reached 90.1 W/m² with an overall reduction of 13.1% in the space daily load. The walls' maximum temperature went down to 28.0 °C yielding a decrease in the peak radiant temperature asymmetry to 0.5 °C. These results constitute a limitation on the proposed system which becomes less efficient when applied in regions suffering from continuous humid weathers.



(a)



(b)

Fig. 10. Hourly distribution of the (a) Space load and (b) Window temperature with and without the system for Jeddah.

CHAPTER VI

CONCLUSION

A passive technique for reducing the temperatures of glazing surfaces is developed in order to decrease the energy consumed in offices space and the resulting radiation asymmetry with respect to nearby occupants. The proposed system combines the principles of passive evaporative cooling and solar chimneys without sacrificing the indoor conditions and requirements. An integrated model consisting of the system applied on the window of a space was developed and validated experimentally. The system was then applied to an office space located in Riyadh and was found to reduce the total load by up 19.4% in spaces having window-to-wall ratios of 40% when clear double pane windows are used. In addition, the system was capable of reducing the sensation of thermal discomfort due to radiation asymmetry with respect to an occupant seated one meter away from the window. However, energy savings of 13.1% were found when the proposed system was applied in Jeddah. The use of the proposed system was found to be limited by the outdoor relative humidity which restricts its benefits in locations suffering from humid weather conditions.

BIBLIOGRAPHY

- [1] Alawadhi E. Effect of an incompletely closed window shutter on indoor illuminance level and heat gain. *Energy and Buildings* 2016;110:112-119.
- [2] Chasar D, Moyer N, Rudd A, Parker D, Chandra S. Measured and simulated cooling performance comparison; insulated concrete form versus frame construction. In proceedings of ACEEE, Washington, DC, USA; August 2002.
- [3] Al-Othmani M, Ghaddar N, Ghali K. A multi-segmented human bioheat model for transient and asymmetric radiative environments. *International Journal of Heat and Mass Transfer* 2008;51:5522-5533.
- [4] Antoun S, Ghaddar N, Ghali K. Coaxial personalized ventilation system and window performance for human thermal comfort in asymmetrical environment. *Energy and Buildings* 2016;111:253-266.
- [5] Kontoleon K. Dynamic thermal circuit modelling with distribution of internal solar radiation on varying façade orientations. *Energy and Buildings* 2012;47:139-150.
- [6] Li C, Tan J, Chow T, Qiu Z. Experimental and theoretical study on the effect of window films on building energy consumption. *Energy and Buildings* 2015;102:129-138.
- [7] Ye H, Long L, Zhang H, Gao Y. The energy saving index and the performance evaluation of thermochromic windows in passive buildings. *Renewable Energy* 2014;66:215-221.
- [8] DeForest N, Shehabi A, Garcia G, Greenblatt J, Masanet E, Lee E, Selkowitz S, Milliron D. Regional performance targets for transparent near-infrared switching electrochromic window glazings. *Building and Environment* 2013;61:160-168.
- [9] Tsikaloudaki K, Laskos K, Theodosiou T, Bikas D. The Energy Performance of Windows in the Mediterranean Regions. *Energy and Buildings* 2015;92:180-187.
- [10] Arici M, Karabay H, Kan M. Flow and heat transfer in double, triple and quadruple pane windows. *Energy and Buildings* 2015;86:394-402.
- [11] Zhong K, Li S, Sun G, Li S, Zhang X. Simulation study on dynamic heat transfer performance of PCM-filled glass window with different thermophysical parameters of phase change material. *Energy and Buildings* 2015;106:87-95.
- [12] Gosselin J, Chen Q. A dual airflow window for indoor air quality improvement and energy conservation in buildings. *HVAC&R Research* 2008;14(3):359-372.
- [13] Chow T, Lin Z, Fong K, Chan L, He M. Thermal performance of natural airflow window in subtropical and temperate climate zones—A comparative study. *Energy Conversion and Management* 2009;50(8):1884-1890.
- [14] Wei J, Zhao J, Chen Q. Energy performance of a dual airflow window under different climates. *Energy and Buildings* 2010;42(1):111-122.
- [15] Bergman T, Incropera F, Lavine A. Fundamentals of heat and mass transfer, chapter 8 -Internal flow. 2002.
- [16] Miyazaki T, Akisawa A, Nikai I. The cooling performance of a building integrated evaporative cooling system driven by solar energy. *Energy and Buildings* 2011;43(9): 2211-2218.
- [17] Itani M, Ghali K, Ghaddar N. Increasing energy efficiency of displacement ventilation integrated with an evaporative-cooled ceiling for operation in hot humid climate. *Energy and Buildings* 2015;105:26-36.

- [18] Kim M, Jeong D, Jeong J. Practical thermal performance correlations for a wet-coil indirect evaporative cooler. *Energy and Buildings* 2015;96:285-298.
- [19] Lee D, Hung T, Lin J, Zhao J. Experimental investigations on solar chimney for optimal heat collection to be utilized in organic Rankine cycle. *Applied Energy* 2015;154:651-662.
- [20] Yassine B, Ghali K, Ghaddar N, Srour I, Chehab G. A numerical modeling approach to evaluate energy-efficient mechanical ventilation strategies. *Energy and Buildings* 2012;55:618-630.
- [21] Vorre M, Jensen R, Le Dréau J. Radiation exchange between persons and surfaces for building energy simulations. *Energy and Buildings* 2015;101:110-121.
- [22] Hagishima A, Tanimoto J. Field measurements for estimating the convective heat transfer coefficient at building surfaces. *Building and Environment* 2003;38(7):873-881.
- [23] Duffie J, Beckman W. *Solar engineering of thermal processes*, chapter 3 – Selected heat transfer topics. 1980.
- [24] Jing H, Chen Z, Li A. Experimental study of the prediction of the ventilation flow rate through solar chimney with large gap-to-height ratios. *Building and Environment* 2015;89:150-159.
- [25] Chen Z, Bandopadhyay P, Halldorsson J, Byrjalsen C, Heiselberg P, Li Y. An experimental investigation of a solar chimney model with uniform wall heat flux. *Building and Environment* 2003;38(7):893-906.
- [26] Sandberg M. Cooling of building integrated photovoltaics by ventilation air. In *Proceedings of the First International One Day Forum on Natural and Hybrid Ventilation*, Sydney, Australia; September 1999.
- [27] Perjési-Hámori I. Simulation of heat radiation asymmetry with maple. 7th International Conference on Mathematical Modelling, Vienna, Australia; February 2012.
- [28] T.G.I Corp. TGI coated glass for architectural application. <http://www.taiwanglass.com>.
- [29] ASHRAE. Standard 62.1 – Ventilation for Acceptable Indoor Air Quality. 2004.
- [30] Fasiuddin M, Budaiwi I. HVAC system strategies for energy conservation in commercial buildings in Saudi Arabia. *Energy and Buildings* 2011;43(12):3457-3466.
- [31] Alaidroos A, Krarti M. Optimal design of residential building envelope systems in the Kingdom of Saudi Arabia. *Energy and Buildings* 2015;86:104-117.
- [32] The Saudi Building Code (SBC)—Section 601: Energy Conservation. 2007.
- [33] The Weather Company, LLC. *Weather Underground*. <https://www.wunderground.com>
- [34] ASHRAE. *Handbook-Fundamentals*, Chapter 14 - Climate Design Information. 2005.
- [35] Zell E, Gasim S, Wilcox S, Katamoura S, Stoffel T, Shibli H, Engel-Cox J, Al Subie M. Assessment of solar radiation resources in Saudi Arabia. *Solar Energy* 2015;119:422-438.

